ELSEVIER

Journal of Alloys and Compounds 218 (1995) 149–156

Journal of ALLOYS AND COMPOUNDS

Study on the development of the lattice strain in $(Mg,U)O_{2+x}$ solid solution

H. Serizawa [a], T. Shiratori [a], K. Fukuda [a], T. Fujino [b], N. Sato [b]

[a] *Japan Atomic Energy Research Institute, Tokai-mura, Naka-Gun, Ibaraki-Ken 319-11, Japan*

[b] *Institute for Advanced Materials Processing, Tohoku University, Sendai 980, Japan*

Received 2 May, 1994

Abstract

Lattice strain observed in magnesia-doped UO_2 was studied. Solid solution $Mg_yU_{1-y}O_{2+x}$ was prepared by the reaction of mixtures of $MgUO_4$, MgU_3O_{10} and UO_2. The composition of the solid solution was analysed by X-ray diffraction (XRD) and electron probe microanalysis. Homogeneous and inhomogeneous strains were evaluated by XRD analysis. The homogeneous strain was explained as caused by the cation defects in the solid solution. The development of the strain was dependent on the number of Mg^{2+}–U^{5+} complexes. The variance method was applied to obtain the inhomogeneous strain. The average crystallite size of the product was also given in the variance analysis. The evolution of the inhomogeneous strain and the decrease in the size of the crystallite were attributed to the precipitation of MgO accompanied by the reduction of the sample.

Keywords: Lattice strain; Magnesium; Uranium

1. Introduction

It is known that Mg dissolves in UO_2, forming the solid solution $Mg_yU_{1-y}O_{2+x}$ in a wide range of Mg contents [1,2]. This solid solution has a CaF_2-type f.c.c. structure with a contracted unit cell, where the Mg^{2+} ion substitutes for the U^{4+} ion in the cation sublattice [3]. Interest in $Mg_yU_{1-y}O_{2+x}$ is attached to the attractive properties of this compound as a potential nuclear fuel. During irradiation, the oxygen potential of the fuel $\Delta\bar{G}_{O_2}$ increases with increasing O/M ratio due to the replacement of fissile atoms by fission products [4]. Although, in the oxygen hyperstoichiometric region, the oxygen potential of $Mg_yU_{1-y}O_{2+x}$ $\Delta\bar{G}_{O_2}$ is significantly higher than that of UO_2, $\Delta\bar{G}_{O_2}$ decreases steeply with decreasing O content, and levels off at a certain O/M ratio in the hypostoichiometric region. It is predicted that the $\Delta\bar{G}_{O_2}$ of $Mg_yU_{1-y}O_{2+x}$ in this range of O/M ratios is low compared with that of stoichiometric UO_2 and the change accompanied by oxygen non-stoichiometry in the solid solution is small [5]. Thus the use of oxygen-poor $Mg_yU_{1-y}O_{2+x}$ as nuclear fuel is expected to depress the oxidation of cladding during irradiation, resulting in the improvement of the irradiation performance.

The formation of the solid solution $Mg_yU_{1-y}O_{2+x}$, has been studied by several researchers. Anderson and Johnson [6] reported that the solubility of MgO in UO_2 was greatly increased by the presence of the extra oxygen which could fill the anion vacancy in the lattice. The solubility of MgO into UO_2 and the phase stability are strongly dependent on the oxygen partial pressure and temperature. When $Mg_yU_{1-y}O_{2+x}$ is prepared by the reaction of magnesium uranates (MgU_3O_{10} and $MgUO_4$) and UO_2 in an He stream which contains oxygen at a relatively high pressure, the y value of the solid solution ranges from 0 to 0.33 [2]. In contrast, the Mg content of the solid solution produced in highly reducing atmosphere was only a few per cent [7]. These results were supported by theoretical calculation of partial molar entropy and enthalpy of the solid solution using the shell model [8].

According to the relationship between the composition and lattice constant [7], the lattice constant of this cubic solid solution varies differently with oxygen content x, in the two regions of negative and positive x values. The inhomogeneous strain caused by the dissolution of Mg was evaluated as a function of Mg content [9]. It has been shown that the inhomogeneous strain was affected by the preparation conditions, especially annealing temperature. We carried out again a series of X-ray diffraction (XRD) measurements on

SSDI 0925-8388(94)01385-3

the $Mg_yU_{1-y}O_{2+x}$ samples with various compositions, and found that the sample with negative x value showed a larger X-ray line broadening compared with that with positive x value, although both of the samples were prepared at the same temperature. This difference suggests that there might be another mechanism which causes the inhomogeneous strain in the solid solution.

In this paper, the two types of lattice strains, i.e. homogeneous strain and inhomogeneous strain, which were observed in the fluorite-type magnesium uranate were discussed separately. The increase in the homogeneous strain was explained with a defect model, which assumes the presence of two kinds of complexes, Mg^{2+}–U^{5+} and Mg^{2+}–$2U^{5+}$, and free Mg^{2+} and U^{5+} ions in the solid solution. The inhomogeneous strain was determined with the aid of broadening analysis of the XRD peak. A crystallite size was also evaluated in the analysis. The root mean square lattice strain and the average crystallite size were evaluated separately by the variance method. The variation of the strain was discussed taking into account the variation of the crystallite size of the solid solution.

2. Experimental details

2.1. Sample preparation

The calculated weights of $MgUO_4$, MgU_3O_{10} and UO_2 were mixed, and the mixture was pressed into pellets 8 mm in diameter. The pellets were first heated at 1300 or 1400 °C in an unpurified He stream for 100 h, where the oxygen concentration of the outlet gas was about 200 ppm. Then the specimens for XRD and electron probe microanalysis (EPMA) were cut out using a diamond wheel. The remaining part of the pellet was washed in ultrasonic cleaning equipment and heated again at the same temperature for 50 h in an atmosphere of He–4%H_2. Each pellet was divided into two parts for XRD analysis and EPMA.

2.2. Composition of the sample

The phase analysis and the determination of the Mg/U ratio were carried out by XRD and EPMA. The oxygen content of the solid solution which was composed of a single phase was determined from the relationship between the lattice constant and the composition [7]. This is different in the two regions of $x \geqslant 0$ and $x < 0$, i.e.

$$a = 0.54704 - 0.00940x - 0.05577y + 0.0055xy \quad (1)$$

$(x \geqslant 0)$ and

$$a = 0.54704 - 0.07095x - 0.05577y \quad (2)$$

$(x < 0)$ where a is the lattice constant of the solid solution, and x and y are the parameters in the chemical formula $Mg_yU_{1-y}O_{2+x}$. The first terms in these equations correspond to the lattice constant of stoichiometric uranium dioxide. For the heterogeneous samples including a precipitate, MgO, the composition of the solid solution $Mg_yU_{1-y}O_{2+x}$ was determined from the relation Eq. (1) or (2) for the lattice parameter obtained by XRD in combination with the Mg concentration in the solid solution which was determined by EPMA. The concentration of Mg in the solid solution can be expressed as

$$N_{Mg} = \frac{M_{Mg}y}{M_{Mg}y + M_U(1-y) + M_O(2+x)} \times 100 \quad (3)$$

where N_{Mg} is the weight per cent of Mg in the solid solution determined by the intensity of characteristic X-rays of Mg in EPMA using a calibration line, and M_{Mg}, M_U and M_O denote the masses of constituent atoms. The composition of the sample was calculated by solving two simultaneous equations, Eq. (1) or (2) and (3).

2.3. Measurement of the XRD line profile

A portion of an $Mg_yU_{1-y}O_{2+x}$ sample cut out from a pellet was powdered and analysed by the XRD method. The XRD line profile of the sample was taken at room temperature using a diffractometer (rotating-anode X-ray tube type RU--200B, Rigaku Co. Ltd.) with Cu Kα radiation monochromated by the (002) plane of curved graphite. The slit range was arranged for 0.15° for both divergence and scatter slits. The lattice constant was obtained by fixed time measurement for the period of 3 s at intervals of 0.05° in diffraction angle 2θ between 15.00° and 135°. In order to evaluate the inhomogeneous strain and the crystallite size, the intensity distribution was measured stepwise at an interval of 0.002° within a range of 1°–3° from the peak centre on both sides. The observed line profile was corrected for polarization factor, and then background correction was conducted by subtracting the intensity measured at angles which were sufficiently distant from the peak position.

3. Calculation

The inhomogeneous strain and the average crystallite size of each sample were determined using the variance or the mean square breadth as a measure of line profile [10–15]. The observed variance is defined with diffraction intensity $I(\theta)$ as

$$W_{2\theta} = \frac{\int (2\theta - \langle 2\theta \rangle)^2 I(2\theta)\, d(2\theta)}{\int I(2\theta)\, d(2\theta)} \quad (4)$$

where $\langle 2\theta \rangle$ is the centroid of the X-ray distribution defined as

$$\langle 2\theta \rangle = \frac{\int 2\theta I(2\theta)\, d(2\theta)}{\int I(2\theta)\, d(2\theta)} \quad (5)$$

The evaluation of the variance depends sensitively on the choice of the background level; it is known that the choice of the beginning and end points of the peak significantly affects the calculated results [11,16]. However, this difficulty can be circumvented by the truncation operation described by Ladell et al. [16]. In this study, the integration limits $2\theta_1$ and $2\theta_2$ were determined with the following conditions:

$$I(2\theta_1) = I(2\theta_2) \quad (6)$$

and

$$\int_{2\theta_1}^{2\theta_2} I(2\theta)\, d(2\theta) - I(2\theta_1)(2\theta_2 - 2\theta_1) = 0.9 \int_{-\infty}^{\infty} I(2\theta)\, d(2\theta) \quad (7)$$

Ladell et al. [16] report that the shape of the X-ray distribution is maintained intact by this procedure.

When the inhomogeneous strain and the small particle size simultaneously cause broadening of the diffraction profile, the observed variance calculated in this manner becomes the sum of three independent terms as

$$W_{2\theta} = W_{2\theta}^{D} + W_{2\theta}^{S} + W_{2\theta}^{I} \quad (8)$$

where $W_{2\theta}^{D}$ and $W_{2\theta}^{S}$ indicate the variances of the lattice strain and the crystallite size respectively. $W_{2\theta}^{I}$ is the variance due to instrumental effects. Wilson has shown that $W_{2\theta}^{D}$ and $W_{2\theta}^{S}$ are given approximately as

$$W_{2\theta}^{D} = 4 \tan^2 2\theta \langle e^2 \rangle \quad (9)$$

and

$$W_{2\theta}^{S} = \frac{K\lambda\Delta(2\theta)}{2\pi^2 p \cos\theta} \quad (10)$$

where K, λ, p, e and $\Delta(2\theta)$ denote the Scherrer constant, the wavelength, the average of the crystallite size, the local strain and the integral width respectively [10,11,13]. The last term $W_{2\theta}^{I}$ is determined with a standard sample. In the present work, $W_{2\theta}^{I}$ was evaluated as a function of diffraction angle 2θ with high purity silicon powder annealed at 850 °C for 50 h. Then the net variance $W_{2\theta}^{SD}$ was obtained by subtracting $W_{2\theta}^{I}$ calculated at the diffraction angle from the observed $W_{2\theta}$. Consequently, $W_{2\theta}^{SD}$ is given in the form [11,13]

$$W_{2\theta}^{SD} = \frac{K\lambda\Delta(2\theta)}{2\pi^2 p \cos\theta} + 4 \tan^2\theta \langle e^2 \rangle \quad (11)$$

4. Results and discussion

4.1. Composition analysis

XRD analysis is not so sensitive to the MgO phase in the sample because of the low scattering factor of the Mg atom compared with the U atom. Thus analysis with EPMA is essential for the study of the phase relation in this system. The typical results of the analyses are given in Figs. 1 and 2. The backscattered electron

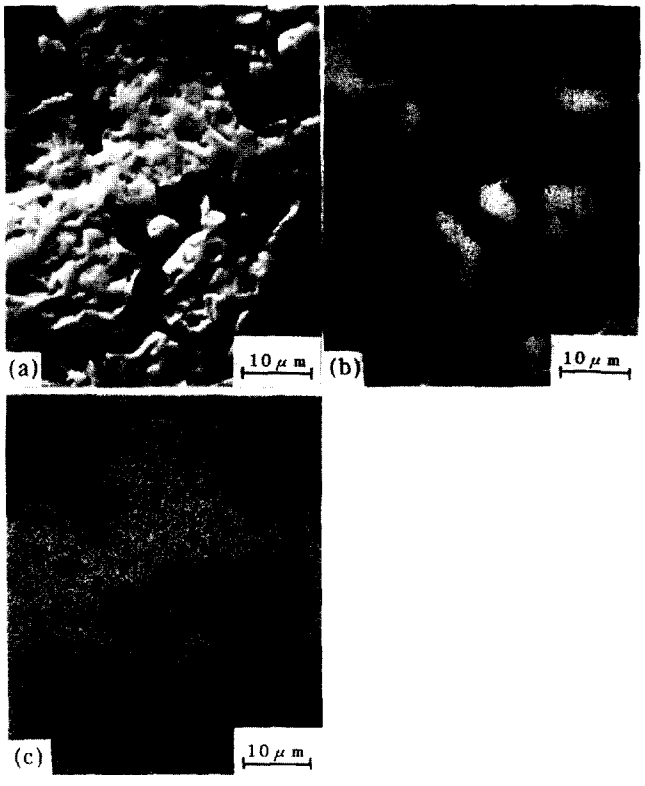

Fig. 1. EPMA of the sample (a)-3: (a) BSE image; (b) X-ray map of Mg atom; (c) X-ray map of U atom.

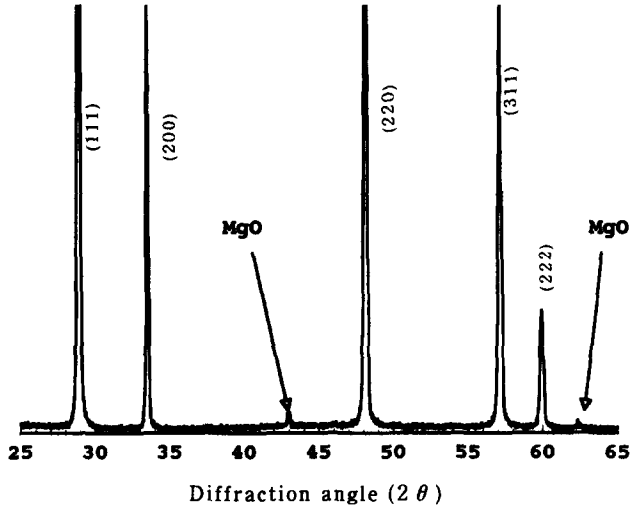

Fig. 2. XRD pattern of the sample (a)-3.

Table 1
Results of the analyses of the samples prepared in this study

Specimen	Initial composition (Mg/metal)	Reaction temperature (°C)	Atmosphere	MgO phase		Lattice constant (nm)	Chemical formula
				XRD	EPMA		
(a)-1	0.10	1300	He	–	–	0.5410	$Mg_{0.1}U_{0.9}O_{2.05}$
(a)-2	0.20	1300	He	–	–	0.5360	$Mg_{0.2}U_{0.8}O_{2.00}$
(a)-3	0.30	1300	He	+ +	+ + +	0.5350	$Mg_{0.22}U_{0.91}O_{1.98}$
(b)-1	0.10	1300	He; He–4%H_2	–	+	0.5460	$Mg_{0.09}U_{0.91}O_{1.94}$
(b)-2	0.20	1300	He; He–4%H_2	+ +	+	0.5460	$Mg_{0.18}U_{0.82}O_{1.87}$
(b)-3	0.30	1300	He; He–4%H_2	+ + +	+ + +	0.5460	$Mg_{0.19}U_{0.81}O_{1.86}$
(c)-1	0.21	1400	He	–	+	0.5384	$Mg_{0.16}U_{0.84}O_{2.00}$
(c)-2	0.15	1400	He	–	+	0.5392	$Mg_{0.14}U_{0.86}O_{2.01}$
(c)-3	0.11	1400	He	–	–	0.5412	$Mg_{0.11}U_{0.89}O_{2.02}$
(c)-4	0.015	1400	He	–	–	0.5461	$Mg_{0.015}U_{0.985}O_{2.01}$
(d)-1	0.21	1400	He; He–4%H_2	+ + +	+ +	0.5466	$Mg_{0.14}U_{0.86}O_{1.90}$
(d)-2	0.15	1400	He; He–4%H_2	+ +	+ +	0.5467	$Mg_{0.13}U_{0.87}O_{1.91}$
(d)-3	0.11	1400	He; He–4%H_2	+	+	0.5466	$Mg_{0.08}U_{0.92}O_{1.94}$
(d)-4	0.015	1400	He; He–4%H_2	–	–	0.5467	$Mg_{0.015}U_{0.985}O_{1.99}$
UO_2	0.0	1300	He; He–4%H_2			0.5470	$UO_{2.00}$

(BSE) image of sample (a)-3 (Table 1) in Fig. 1 reveals the presence of a grey phase surrounded by brighter regions. The X-ray images in the figure show that the Mg atom is concentrated in the former phase. This segregated phase was identified as MgO by the XRD line profile given in Fig. 2. The X-ray images of the sample show that the Mg atom in UO_2 distributes homogeneously to form uniform solid solution. The principal features of the products analysed by XRD and EPMA are summarized in Table 1. It seems that the O content in the solid solution decreases with increasing Mg content. Comparing the samples prepared at 1300 °C with those prepared at 1400 °C, it is clear that the solubility of Mg in UO_2 decreases with increasing temperature.

According to Ref. [2], the maximum y value of $Mg_yU_{1-y}O_{2+x}$ obtained at 1300 °C in the He stream was about 0.3. However, in the present work, the solubility of Mg into $Mg_yU_{1-y}O_{2+x}$ phase produced in He atmosphere was remarkably low compared with the results of the reference. The oxygen partial pressure of $Mg_yU_{1-y}O_{2+x}$ may increase with increasing y value because of the decrease in $\Delta\bar{S}_{O_2}$ [2]. Consequently, this difference might be attributable to the lower oxygen pressures in the present study.

4.2. Homogeneous lattice strain in the solid solution

The lattice constant of $Mg_yU_{1-y}O_{2+x}$ varies not only with y value but also with x value [7]. It is interesting that the x value dependence of the lattice constant in the oxygen hyperstoichiometric region is much smaller than that in the oxygen hypostoichiometric region [7]. It is generally known that the Mg ions which are dissolved into UO_2 substitute at the lattice site of U ions in forming the solid solution. Since the valence state and the ionic radius of Mg^{2+} are considerably different from those of the U ion, it might be reasonable that the distortion of the U ions around the Mg impurity centre is so great that homogeneous lattice strain takes place, which results in the variation of the lattice constant.

The formation of the defects on dissolution of Mg into UO_2 can be predicted as follows. Aronson and Clayton applied a defect model involving localized electronic disorder to both UO_2 and $(U,Th)O_{2+x}$ [17]. In UO_2 with the fluorite structure, the valence states of oxygen and uranium are -2 and $+4$, respectively. When a cation in the divalent state dissolves and replaces a uranium ion in the crystal, this cation is considered as a -2-charged defect and the oxidized neighbouring uranium ions which exhibit $+5$ valences are regarded as $+1$-charged defects [5]. The attractive interaction between these negative and positive defects can cause the formation of Mg^{2+}–αU^{5+} complexes, where α denotes the average number of U^{5+} ions in the complex ($1<\alpha<2$) [5]. Also, there are free Mg^{2+} and free U^{5+} ions which do not take part in the formation of the complex. The oxygen potential of $M_yU_{1-y}O_{2+x}$ interpreted by their model was in harmony with the experimental results.

The number of defects of each type can be determined by the mass action low [5]. In Fig. 3, the numbers of defect complexes and cation defects per mole of solid solution are given as a function of O content. Since the α value for $Mg_yU_{1-y}O_{2+x}$ was not available, for a rough estimation the value was taken to be the same as in $Eu_yU_{1-y}O_{2+x}$, 1.66 which was determined experimentally [5]. As can be seen in the figures, it is convenient to discuss the formation of defects by dividing

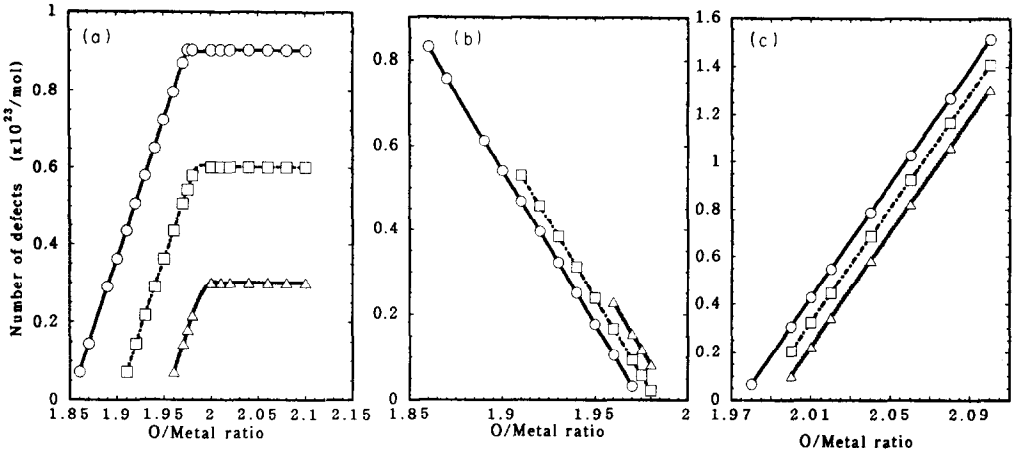

Fig. 3. Variation of the number of defects in 1 mol of the solid solution: (a) defect complex; (b) free Mg^{2+} ion; (c) free U^{5+} ion; ○, Mg/metal ratio = 0.15; □, Mg/metal ratio = 0.10, △, Mg/metal ratio = 0.05.

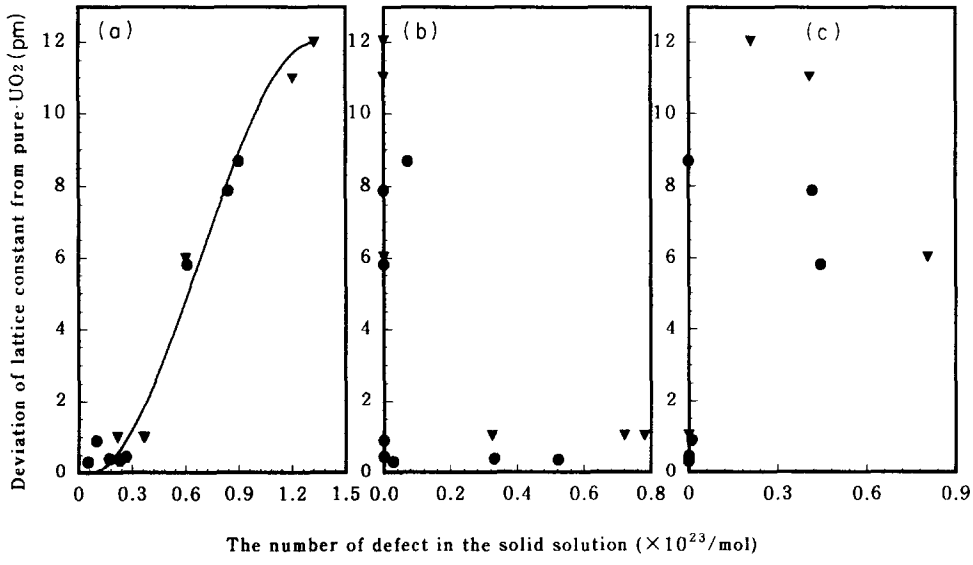

Fig. 4. Relationships between the number of defects and the variation of the lattice constant: (a) defect complex; (b) free Mg^{2+} ion; (c) free U^{5+} ion; ▼ specimens prepared at 1300 °C; ●, specimens prepared at 1400 °C.

the oxygen non-stoichiometry into two regions. The boundary between the two regions is calculated by the relation $x_{boundary} = 2-(1-\alpha/2)y$ (in this case, $x_{boundary} = 1.99$, $x_{boundary} = 1.98$ and $x_{boundary} = 1.97$ for $y = 0.05, y = 0.10$ and $y = 0.15$ respectively) [5]. The defect complex Mg^{2+}–αU^{5+} is present in both of the two regions, whereas the free ion kind of defect is strongly dependent on the O content. In the oxygen-poor region ($x < x_{boundary}$), there are free Mg^{2+} ions in addition to the complexes. The number of free Mg^{2+} ions which do not combine with U^{5+} ions decreases steeply with increasing O content, and this Mg^{2+} ion almost vanishes in the vicinity of $x_{boundary}$. In the oxygen-rich region ($x_{boundary} < x$), the Mg^{2+} ions are completely consumed to form Mg^{2+}–αU^{5+}; but the excess U^{5+} ions remain free. The number of U^{5+} ions increases with increasing O content. The relationship between the lattice defects and the development of the homogeneous strain can be clarified by plotting the deviation of the lattice constant as a function of the number of defects of each type per mole of the solid solution. The plots given in Fig. 4 show that the deviation of the lattice constant increases as the number of defect complexes increases, indicating that the homogeneous lattice strain of the solid solution is greatly affected by the formation of the Mg^{2+}–αU^{5+} complex. The effect of the presence of other types of defects on the homogeneous strain can be neglected compared with that of the defect complex. Of course, the effect of oxygen non-stoichiometry on the lattice strain cannot be neglected; it is, however, taken into account indirectly in the model because the oxygen content is, as described above, one of the parameters used to calculate the number of lattice defects.

4.3. Inhomogeneous strain and crystallite size

The purpose of the peak broadening analysis is to get information on the variation of the crystallinity of this ceramic compound in two separate terms of inhomogeneous strain and particle size in relation to the preparation condition of the solid solution. Fig. 5 illustrates the measured (620) profile of samples (a)-2 and (b)-2. A marked peak broadening is observed in the profile of sample (b)-2, which was prepared by the reduction of sample (a)-2. This figure implies that the crystallinity of the sample depends on some factors other than the reaction temperature. Similar results were observed for all the samples which were heat treated in He–4%H_2.

Fig. 6 illustrates $W_{2\theta}{}^{SD} \cos\theta/\Delta(2\theta)\lambda$ plotted against $4 \sin\theta \tan\theta/\Delta(2\theta)\lambda$ for sample (b)-1 as an example. The broken line results from the reflections from (200) and (400) planes, and the solid line is calculated using other planes of reflection. Taking the x axis as $4 \sin\theta \tan\theta/\Delta(2\theta)\lambda$ and y axis as $W_{2\theta}{}^{SD} \cos\theta/\Delta(2\theta)\lambda$, the y axis intersection of the line gives $K/2\pi^2 p$ and the slope of the line $\langle e^2 \rangle$ which designates the inhomogeneous strain. As can be seen in Fig. 6, the intersection of the y axis with the dotted line is somewhat smaller than that with the solid line. In contrast, the slopes of the two lines which indicate the strain are well consistent with each other. The ratio of the average crystallite size $p_{100}/p_{\text{other direction}}$ was, however, almost

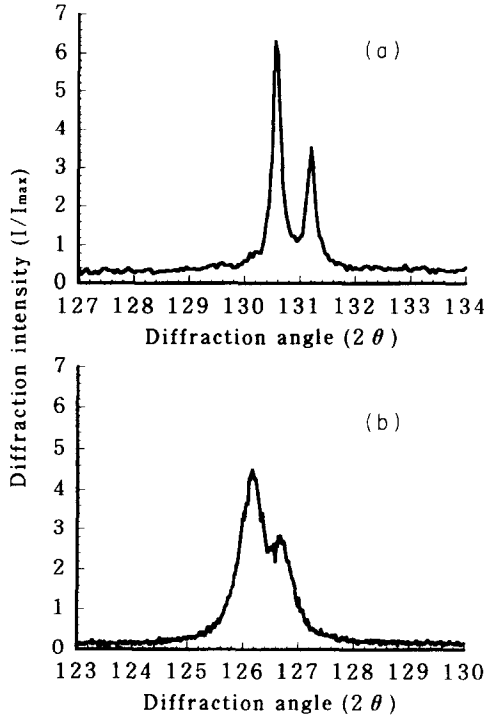

Fig. 5. Measured (620) diffraction profiles of the sample: (a) sample (a)-2 (prepared in He atmosphere at 1300 °C); (b) sample (b)-2 (sample of (a)-2 reduced in He–4%H_2 at 1300 °C).

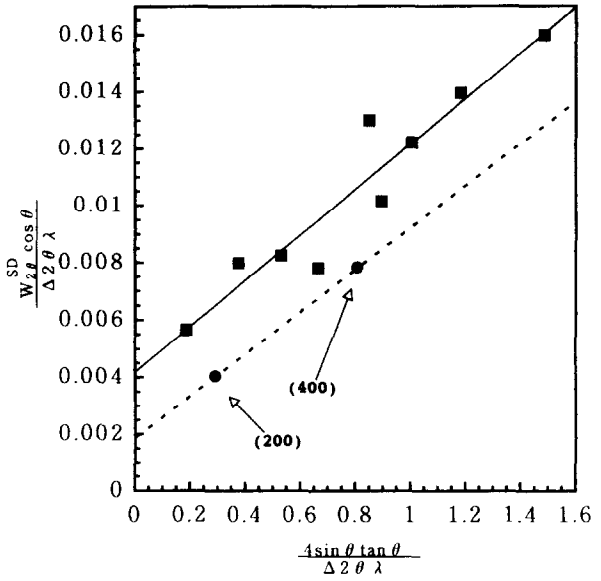

Fig. 6. Dependence of $W_{2\theta}{}^{SD} \cos\theta/\Delta(2\theta)\lambda$ on $4 \sin\theta \tan\theta/\Delta(2\theta)\lambda$: ●, calculated point for reflection from (h00); ■, calculated point for reflection from the other planes.

the same in all samples. This means that the difference in the intersection of the y axis might be due to the Scherrer constant K for the reflection rather than the anisotropy of the sample [11,18]. Therefore the mean size and strain parameter were calculated using all reflections other than the (h00) planes. In order to confirm the reliability of this analysis, the diffraction data of a pure UO_2 sample were analysed using this method. The sample was prepared by heat treatment at 1300 °C in He–4%H_2. The O/U ratio of the sample estimated with the lattice constant was 2.00 and the broadening of the peak was not observed, indicating that the sample had a CaF_2-type f.c.c. structure with no lattice strain. The analysis showed that the strain of this standard sample was less than 10^{-4}. The mean crystallite size was about 150 nm. Although the crystallite size of UO_2 should be dependent on the preparation conditions, this is in good agreement with the reported values within the scattering of the data [19,20]. This result suggests that the variance method is effective for the evaluation of the lattice strain and crystallite size of this kind of isotropic ceramic compound.

In Fig. 7, the inhomogeneous lattice strain of the solid solutions is plotted as a function of the composition. The calculated distortion of the solid solution is much larger than that of pure UO_2. In Fig. 7(a), the relationship between the strain and Mg content is shown. It is evident that the inhomogeneous strain detected in the samples prepared in strongly reducing atmosphere (He–4%H_2) is larger than that observed in the sample heat treated in He atmosphere. The strain plotted against O/metal ratio is given in Fig. 7(b). As shown in this figure, the inhomogeneous strain increases with decreasing O/metal ratio of the solid solution. The

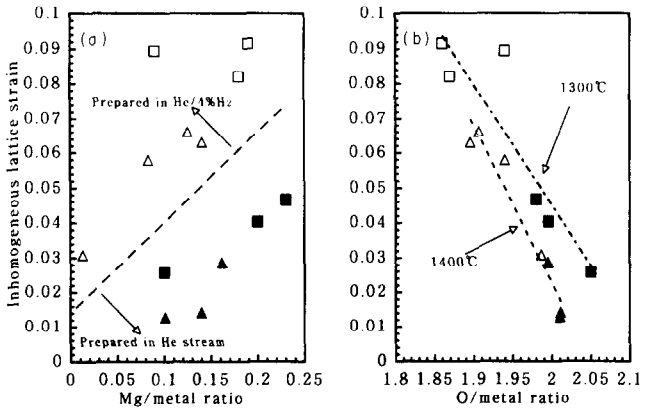

Fig. 7. Observed inhomogeneous strain as a function of the composition: ■, the samples prepared at 1300 °C in He atmosphere; □, the samples heat treated in He–4%H_2 atmosphere; ▲, the samples prepared at 1400 °C in He atmosphere; △, the samples heat treated in He–4%H_2 atmosphere.

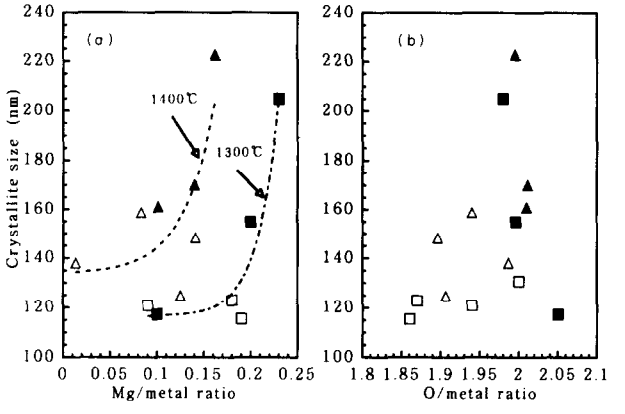

Fig. 8. Measured crystallite size of the solid solution as a function of the composition: ■, the samples prepared at 1300 °C in He atmosphere; □, the samples heat treated in He–4%H_2 atmosphere; ▲, the samples prepared at 1400 °C in He atmosphere; △, the samples heat treated in He–4%H_2 atmosphere.

lattice distortion of $Mg_yU_{1-y}O_{2+x}$ was reported to be affected by the preparation temperature [9]. It is evident here that the magnitude of the inhomogeneous strain greatly depends on the annealing temperature. Our results in Fig. 7(b) also show that the inhomogeneous strain decreases with increasing temperature, but the inclination to develop the strain with decreasing O content is independent of its reaction temperature. One possible explanation for this change of the inhomogeneous strain with O/M ratio is that the precipitate of MgO evolved as the decrease of the oxygen potential caused the inhomogeneous strain.

The mean values of the crystallite size were found to be in the range 100–250 nm which was comparable with the reported value [3]. Though the data plotted in Fig. 8(a) show some scatter, the crystallite size of the sample produced in He atmosphere (represented by the full square symbol) seems to increase with increasing Mg content. The previous work by Ingleby and Hand [21] pointed out the rapid grain growth of Mg-doped UO_2. There might be some relationships between the grain growth and the increase in the crystallite size. In the figure, the temperature dependence of the crystallite size is shown. The size increases with increasing preparation temperature of the solid solution.

Fig. 8(b) depicts the variation of the crystallite size of the solid solution with O/M ratio. It should be noted that the crystallite size decreases when the samples are reduced. In other words, the figure indicates that the crystallite of the solid solution is subdivided by the precipitation of MgO, which would cause the inhomogeneous stress detected in the present work.

5. Summarizing remarks

This work indicated that the maximum y value of the solid solution $Mg_yU_{1-y}O_{2+x}$ was about 0.22 under the present experimental conditions, and was decreased by the heat treatment in He–4%H_2 atmosphere.

The homogeneous lattice strain was evaluated and correlated to the defects in the solid solution using the cation–cation defect model of the CaF_2-type structure. It was found that the variation of the magnitude of the homogeneous strain was attributed to the presence of the defect complex Mg^{2+}–αU^{5+}. It was also confirmed that both the magnitude of the inhomogeneous strain and the size of the crystallite were dependent on the preparation temperature of the solid solution. The development of the inhomogeneous strain and the decrease in the crystallite size which did not depend on the preparation temperature were considered to be ascribed to the precipitation of MgO generated during the heat treatment in He–4%H_2.

Acknowledgements

The authors are greatly indebted to Mr. K. Ito (Japan Atomic Energy Research Institute (JAERI)) for his skillful cooperation and Dr. K. Minato, Dr. T. Ogawa and Mr. Y. Ishii (JAERI) for extensive discussion. They also wish to express their thanks to Dr. E. Tachikawa, Dr. M. Handa (JAERI) and Dr. S. Yamanaka (Osaka University) for their interest and encouragement.

References

[1] S. Kemmler-Sack and W. Rudroff, *Z. Anorg. Allg. Chem.*, *354* (1967) 255.
[2] T. Fujino and K. Naito, *J. Inorg. Nucl. Chem.*, *32* (1970) 627.
[3] T. Fujino, *J. Inorg. Nucl. Chem.*, *34* (1972) 1563.
[4] H. Holleck and H. Kleykamp, *German Rep. KFK-1181*, 1970.
[5] T. Fujino and N. Sato, *J. Nucl. Mater.*, *189* (1992) 103.

[6] J.S. Anderson and K.D.B. Johnson, *J. Chem. Soc.*, (1953) 1731.
[7] T. Fujino, J. Tateno and H. Tagawa, *J. Solid State Chem., 24* (1978) 11.
[8] M. Sugisaki, *J. Nucl. Mater., 79* (1979) 338.
[9] T. Fujino, *J. Inorg. Nucl. Chem., 34* (1972) 1563.
[10] A.J.C. Wilson, *Proc. Phys. Soc., London, 80* (1962) 286.
[11] H.P. Klug and L.E. Alexander, *X-ray Diffraction Procedures for Polycrystalline and Amorphous Materials*, Wiley, New York, 1974, p. 618.
[12] A.J.C. Wilson, *Mathematical Theory of X-ray Powder Diffractometry*, Philips Technical Library, 1963, p. 94.
[13] N.C. Halder and C.N.J. Wagner, in Gavin R. Mallet, Marie Fay and William M. Mueller (eds.), *Advances in X-ray Analysis*, Vol. 9, Plenum Press, New York, 1966, p. 91.
[14] A.J.C. Wilson, *J. Appl. Crystallogr., 4* (1971) 440.
[15] R.B. Roof, Jr., in Kurt F.J. Heinrich, Charles S. Barrett, John B. Newkirk and Clayton O. Ruud (eds.), *Advances in X-ray Analysis*, Vol. 15, Plenum Press, New York, 1972, p. 307.
[16] J. Ladell, W. Parrish and J. Taylor, *Acta Crystallogr., 12* (1959) 561.
[17] S. Aronson and J.C. Clayton, *J. Chem. Phys., 32* (1960) 749.
[18] J.I. Langford and A.J.C. Wilson, *J. Appl. Crystallogr., 11* (1978) 102.
[19] H.G. Riella, L.G. Martinez and K. Imakuma, *J. Nucl. Mater., 153* (1988) 71.
[20] C.S. Choi, J.H. Park, E.H. Kim, H.S. Shin and I.S. Chang, *J. Nucl. Mater., 153* (1988) 148.
[21] B.E. Ingleby and K. Hand, Fission product behavior in ceramic oxide fuel, *Proc. American Ceramic Society Annu. Meet., 1986* p. 57.